Impact of Inter-core Crosstalk on the Performance of Multi-core Fibers-based SDM Systems with Coherent Detection

Bruno R. P. Pinheiro, João L. Rebola and Adolfo V. T. Cartaxo
Optical Communications and Photonics Group, Instituto de Telecomunicações, Lisboa, Portugal
Instituto Universitário de Lisboa (ISCTE-IUL), Lisboa, Portugal

Keywords: Inter-core Crosstalk, Monte-Carlo Simulation, Multi-core Fibers, Optical Coherent Detection, Space-division Multiplexing.

Abstract: Inter-core crosstalk (ICXT) can limit the multi-core fiber (MCF) systems performance and transmission reach. Over the last years, the impact of the ICXT on the performance of MCF optical communication systems with coherent detection has been investigated in several works. However, the influence of the MCF parameters and transmitted signal characteristics on the ICXT mechanism and the degradation induced by it on the performance of coherent detection MCF systems are still to be completely assessed. In this work, the impact of the ICXT on the performance of coherent detection MCF-based transmission systems is assessed through numerical simulation considering fiber linear propagation. The metrics used to assess the MCF system performance are the bit error rate (BER) and the optical signal-to-noise ratio (OSNR) penalty due to the ICXT. Our results show that the BER and the OSNR penalty due to the detected ICXT, in MCF-based systems with coherent detection, are influenced by the skew, time misalignment between the transmitted signals and the roll-off factor of the transmitted signals. In the range of skew and roll-off factors analyzed, the maximum reduction of maximum ICXT level for a 1 dB OSNR penalty by appropriate choice of skew and roll-off factor does not exceed 1.7 dB.

1 INTRODUCTION

Current long-haul optical networks based on standard single-mode single-core fibers (SMFs) can no longer respond efficiently to the exponential rapid traffic growth. Thereby, in order to respond to the ever-growing traffic demand, new technologies are required to reach higher capacities on the optical communication systems (Klaus et al., 2017). Space division multiplexing (SDM) has been proposed as a solution to achieve higher capacity in future long-haul optical networks (Klaus et al., 2017). The implementation of SDM is based on two main approaches, which consist basically on using two different types of fiber (Saitoh and Matsuo, 2016). The first type of fiber is known as few-mode fiber (FMF) and makes use of several propagation modes in the fiber as transmission channels. The main drawback of FMFs is the requirement of a multi-input multi-output (MIMO) digital signal processing (DSP) receiver to minimize the group delay spread between the different modes. Furthermore, the FMF limits the exploitation of the space domain, except for enhanced capacity-transmission reach, since all modes must be received as a single entity (Klaus et al., 2017). The second fiber type is the multi-core fiber (MCF), in which, independent channels are transmitted in different cores inside the fiber. Thereby, the signals transmitted in each core of the MCF can have different symbol rates, different modulation formats and different temporal misalignments between them. In homogeneous MCFs, the relative uniformity of the cores supports multi-dimensional spatial channels that enable shared transmitter and receiver hardware, simplified DSP and switching (Cartaxo et al., 2016). The use of MCFs has been proposed for several optical communication networks such as access, long-haul, intra-data centers and radio-over-fiber based networks (Puttnam et al., 2017), and so, in this work, we restrain our studies only to MCF-based optical communication system.

As optical coherent detection with polarization-division multiplexing (PDM) is the selected detection technology of actual backbone optical networks (Xia and Wellbrock, 2013), the majority of the MCF-based SDM systems tested so far, consider coherent detection (Puttnam et al., 2017): in 2011, a high-capacity transmission experiment reached 112 Tbps capacity using a MCF with 7 cores and transmitting

Pinheiro, B., Rebola, J. and Cartaxo, A.
Impact of Inter-core Crosstalk on the Performance of Multi-core Fibers-based SDM Systems with Coherent Detection.
DOI: 10.5220/0006623400740081
In *Proceedings of the 6th International Conference on Photonics, Optics and Laser Technology (PHOTOPTICS 2018)*, pages 74-81
ISBN: 978-989-758-286-8

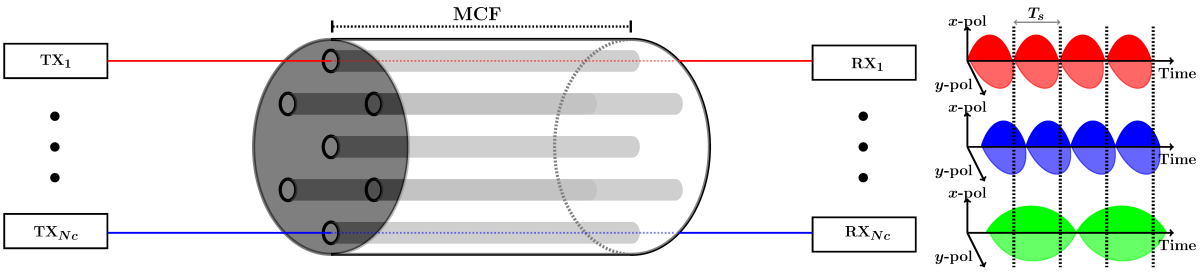

Figure 1: Schematic of the MCF-based SDM system with Nc transmitters (TX_1 to TX_{Nc}) and the respective receivers (RX_1 to RX_{Nc}). The signals transmitted in each core are multiplexed on the polarization.

PDM-QPSK signals (Zhu et al., 2011). By the end of 2012, a 12 core MCF experiment exceeded 1 Pbps capacity (Takara et al., 2012). In 2015, it was reported that a 22-core homogeneous MCF demonstration exceeded 2 Pbps (Puttnam et al., 2015). It is expected that MCFs can attain a transmission capacity beyond 10 Pbps (Morioka, 2017). MCF transmission with coherent detection is definitely the most promising transmission technology that will allow to increase substantially the transmission capacities of the actual long-haul optical networks and to implement SDM optical networks with low complexity.

However, an important limitation of the performance of the weakly-guided MCFs is the inter-core crosstalk (ICXT) (Fini et al., 2010; Rademacher et al., 2017a; Hayashi et al., 2014; Rademacher et al., 2017b). ICXT arises in homogeneous MCFs which have cores with similar properties. ICXT can be reduced by increasing the distance between cores. However, maintaining the same cladding diameter, this method can lead to the reduction of the number of cores, thus, reducing the overall transmission capacity (Hayashi et al., 2013; Hayashi et al., 2011). Over the last years, the ICXT has been researched and some relevant conclusions have been drawn concerning the mechanism of the ICXT and its influence on the performance of the MCF-based SDM systems (Hayashi et al., 2014; Cartaxo et al., 2016). In (Hayashi et al., 2014), a theoretical model of ICXT is proposed and the impact of the ICXT on the performance of the MCF transmission systems is assessed theoretically. In (Cartaxo et al., 2016), the ICXT model presented in (Hayashi et al., 2014) is extended, by considering the ICXT dependence on the group velocity dispersion and the skew between cores. In addition, the transfer function of the ICXT field is derived for homogeneous MCF. This transfer function helps to study the influence of the ICXT on the performance degradation of MCF-based optical systems with walk-off between fiber cores (skew), slightly different group velocities between cores, and by considering different modulation formats (as the typically ones used for coherent detection) at the MCF input.

In this work, we assess numerically through Monte-Carlo (MC) simulation, the influence of the ICXT on the bit error rate (BER) and the optical signal-to-noise (OSNR) penalty of the MCF-based optical communication system with coherent detection, considering 4-Quadrature Amplitude Modulation (QAM) signals, with different roll-off factors, different skews and different signal time misalignments between MCF cores.

This work is organized as follows. Section 2 describes the equivalent simulation model used to characterize the MCF-based optical communication system with coherent detection and the ICXT impact on its performance. The validation of the transfer function used in this work to emulate the ICXT behavior on the MCF-based SDM system is performed in section 3. In section 4, the performance of the MCF-based SDM system with coherent detection impaired by ICXT estimated through MC simulation is analyzed. The conclusions are outlined in section 5.

2 MCF-BASED SDM SYSTEM MODEL

Figure 1 depicts schematically a MCF-based optical communication system, with dedicated transmitter and receiver hardware for each core. On the transmitter side, several different signals are launched in the MCF by Nc different transmitters, TX_1 to TX_{Nc}, with Nc corresponding to the number of cores used. Remark that it is assumed that these transmitters generate independent SDM PDM-M-QAM signals, where M is the modulation format order. The PDM-M-QAM signals are propagated through the MCF and are detected individually by Nc optical coherent receivers, RX_1 to RX_{Nc}. Core-coded modulation or polarization core-coded modulation is not considered, since the characterization of the ICXT impact on the performance of MCFs with independent transmission of PDM-M-QAM signals in each core is not fully understood (Rademacher et al., 2017a). On the right

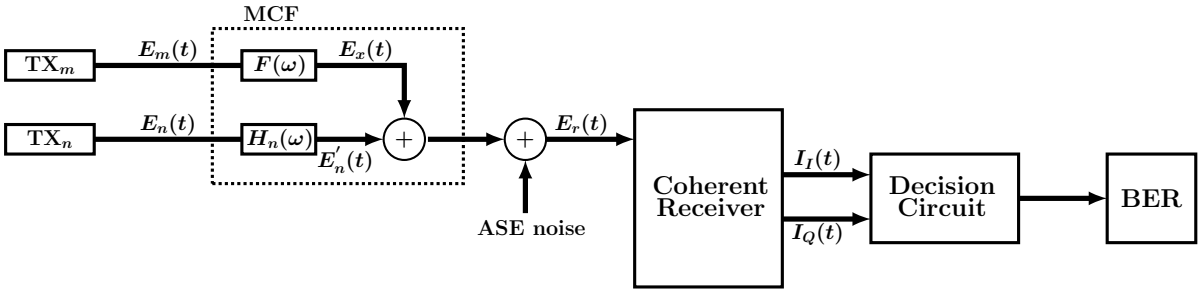

Figure 2: Equivalent simulation model for the MCF-based SDM system, considering single polarization transmission.

hand side of Figure 1, some of the detected PDM-M-QAM signals in each core are depicted illustratively. Since, each core works as a transmission channel independent of the other cores, each transmitted signal can have different symbol rates, different modulation formats and different temporal misalignments between them.

Figure 2 depicts the equivalent simulation model of MCF-based SDM with coherent detection considering single polarization transmission and only two cores. The interfered core is the core n and the interfering core is the core m. The performance of a PDM system with optical coherent detection can be assessed by evaluating only one signal polarization as long as ideal PDM is assumed (Essiambre et al., 2010). Moreover, we assume ideal compensation of the chromatic dispersion at the coherent receiver output. The detected signals have a raised-cosine (RC) pulse shape in order to eliminate the inter-symbol interference at the decision circuit. The RC signals can be generated by making use of the RC filter, which transfer function, $H_{RC}(f)$, is (Carlson and Crilly, 2009)

$$H_{RC}(f) = \begin{cases} T_s & 0 \le |f| \le \frac{1-\beta}{2T_s} \\ T_s \cos^2\left[\frac{\pi T_s}{2\beta}\left(|f| - \frac{1-\beta}{2T_s}\right)\right] & \frac{1-\beta}{2T_s} \le |f| \le \frac{1+\beta}{2T_s} \\ 0 & |f| > \frac{1+\beta}{2T_s} \end{cases} \quad (1)$$

where T_s is the symbol period and β is the roll-off factor. Alternatively, the RC signals can be obtained by having root raised-cosine (RRC) filters at the transmitter and at the receiver, in such a way that $h_{RRC}(t) * h_{RRC}(t) = h_{RC}(t)$, where * is the convolution operator (Carlson and Crilly, 2009). Hence, the transfer function of the RRC filter is $H_{RRC}(f) = \sqrt{H_{RC}(f)}$.

The transmitter output signal of the core n, $E_n(t)$, with RRC pulse shape, can be expressed by

$$E_n(t) = \sqrt{P_n} \sum_{i=-\infty}^{+\infty} (a_{I,i} + j a_{Q,i}) h_{RRC}(t - iT_s) \quad (2)$$

where $a_{I,i}$ and $a_{Q,i}$ are the amplitude of the in-phase (I) and quadrature (Q) components of the i-th M-QAM transmitted symbol, respectively, and P_n is the average power of the transmitted signal at core n. The transmitted signal at core m, $E_m(t)$ is expressed as

$$E_m(t) = \sqrt{P_m} \sum_{i=-\infty}^{+\infty} (a_{I,i}^{(m)} + j a_{Q,i}^{(m)}) h_{RRC}(t - iT_s - \tau_{mn}) \quad (3)$$

where P_m is the average power of the transmitted signal at core m, $a_{I,i}^{(m)}$ and $a_{Q,i}^{(m)}$ are the I and Q components of the i-th M-QAM transmitted symbol of $E_m(t)$, respectively. The amplitude levels, $a_{b,i}$ and $a_{b,i}^{(m)}$, $\forall\, b \in \{I, Q\}$ are random variables that take on equally likely the following values:

$$a_{b,i} \in \{\pm 1, \pm 3, ..., \pm\sqrt{M} - 1\}A \quad (4a)$$

$$a_{b,i}^{(m)} \in \{\pm 1, \pm 3, ..., \pm\sqrt{M} - 1\}A^{(m)} \quad (4b)$$

where A and $A^{(m)}$ are amplitudes that are defined in order that the powers corresponding to the fields $E_n(t)$ and $E_m(t)$ are P_n and P_m, respectively. τ_{mn} is the temporal misalignment between $E_m(t)$ and $E_n(t)$, that takes values between 0 and T_s. The temporal misalignment is the difference between the signal transmission time instants of the each transmitter with reference to the interfered core, i.e., the core in which the receiver performance is assessed.

The propagation in core n is characterized by the transfer function $H_n(\omega) = e^{-j\beta_n(\omega)L}$, where β_n is the propagation constant of core n and L is the length of the MCF. The resulting signal after propagation in the n-th core, $E_n'(t)$, is described by $E_n'(t) = E_n(t) * \mathfrak{F}^{-1}[H_n(\omega)]$ (Agrawal, 2010), where $\mathfrak{F}^{-1}[\,]$ is the inverse Fourier transform operator.

The equivalent simulation model of the MCF to characterize the ICXT between cores m and n is defined by the ICXT field transfer function $F(\omega)$ given by (Cartaxo et al., 2016)

$$F(\omega) = -jK_{nm} e^{-j\beta_n(\omega)L} \sum_{k=1}^{N} e^{-j\Delta\beta_{mn}(\omega)z_k} e^{-j\phi_k} \quad (5)$$

where K_{nm} is the discrete coupling coefficient between cores m and n, N is the number of phase-matching points (PMPs), and ϕ_k is the random phase

shift, introduced at the k-th center point (with longitudinal coordinate z_k) between consecutive PMPs, that is distributed uniformly between 0 and 2π (Cartaxo and Alves, 2017). In Equation (5), $\Delta\beta_{mn}$ is the difference between the propagation constants of core m and n, given by

$$\Delta\beta_{mn}(\omega) = \Delta\beta_{0,mn} + d_{mn}\omega - \frac{1}{2}\frac{\Delta D_{mn}\lambda^2}{2\pi c}\omega^2 \quad (6)$$

In Equation (6), c is the speed of light in vacuum, λ is the wavelength, $\Delta\beta_{0,mn}$ is the difference of the propagation constants at zero frequency, ΔD_{mn} is the difference between the dispersion parameters of core m and n, and d_{mn} is the walkoff between cores m and n, defined by $d_{mn} = \nu_{gm}^{-1} - \nu_{gn}^{-1}$, with ν_{gm} and ν_{gn} being the group velocities in cores m and n, respectively. In this work, we assume that $\Delta\beta_{0,mn}$ and ΔD_{mn} are 0. Hence, Equation (5) is rewritten as

$$F(\omega) = -jK_{nm}e^{-j\beta_n(\omega)L}\sum_{k=1}^{N} e^{-j\omega S_{mn}z_k/L}e^{-j\phi_k} \quad (7)$$

where S_{mn} denotes the skew between the cores m and n and is given by $d_{mn}L$.

The ICXT signal at the output of core n due to the signal in core m, $E_x(t)$, is given by

$$E_x(t) = -jK_{nm}\sqrt{P_m}\left[\sum_{k=1}^{N}[\cos\phi_k - j\sin\phi_k]\cdot \sum_{i=-\infty}^{+\infty}\left[a_{I,i}^{(m)} + ja_{Q,i}^{(m)}\right]h_{RRC}(t - iT_s - S_{mn}z_k/L - \tau_{mn})\right] * \mathfrak{F}^{-1}[H_n(\omega)] \quad (8)$$

After the MCF, the amplified spontaneous emission (ASE) noise is added to the interfered and the ICXT signals. The ASE noise is generated from the optical amplification and is an additive white Gaussian noise with a singlesided power spectral density in each polarization, N_0, defined as $2P_n/(\mathrm{OSNR}\,B_{sim})$, where $2P_n$ is the total average signal power summed over the two states of polarization and B_{sim} is the bandwidth used in the MC simulation (Jeruchim et al., 2000). From this definition, the optical signal-to-noise ratio (OSNR) is defined as the ratio between the total signal power and the total ASE noise power and it is estimated at the coherent receiver input.

Figure 3 depicts the model of a coherent receiver with a 2x4 90° hybrid for a single-polarization transmission (Essiambre et al., 2010). The main goal of the 2x4 90° hybrid is to combine the local oscillator signal, $E_{LO}(t)$, with the incoming signal, $E_r(t)$. The optical fields at the output of the 2x4 90° hybrid are given by (Essiambre et al., 2010)

$$\begin{bmatrix} E_1(t) \\ E_2(t) \\ E_3(t) \\ E_4(t) \end{bmatrix} = \frac{1}{2}\begin{bmatrix} 1 & -1 \\ j & j \\ j & -1 \\ -1 & j \end{bmatrix}\begin{bmatrix} E_r(t) \\ E_{LO}(t) \end{bmatrix} \quad (9)$$

where $E_r(t) = E_n^{'}(t) + E_x(t) + E_{ASE}(t)$. In this work, we assume an ideal synchronization (in time, carrier frequency, phase and polarization) between the LO and the received signals. We also assume that the signal, ICXT and the ASE noise are perfectly aligned in the polarization.

The coherent receiver detects the I and Q components of the incoming signal and then, each IQ component is filtered by $H_{CR}(f)$, which impulse response is $h_{RRC}(t) * h_{cdc}(t)$. This block has two main goals: perform RRC filtering and ideally compensate chromatic dispersion using the filter with impulse response $h_{cdc}(t)$. The ideal balanced photodetectors, placed at the 2x4 90° hybrid output, are modeled as square-law devices. Hence, following the configuration of the coherent receiver depicted in Figure 3, $I_I(t)$ and $I_Q(t)$ are expressed by

$$I_I(t) = \Re\{E_n^{'}(t)E_{LO}^{*}(t) + E_x(t)E_{LO}^{*}(t) + E_{ASE}(t)E_{LO}^{*}(t)\} * h_{CR}(t) \quad (10a)$$

$$I_Q(t) = \Im\{E_n^{'}(t)E_{LO}^{*}(t) + E_x(t)E_{LO}^{*}(t) + E_{ASE}(t)E_{LO}^{*}(t)\} * h_{CR}(t) \quad (10b)$$

where $\Re\{Z\}$ and $\Im\{Z\}$ are, respectively, the real and the imaginary parts of a complex number Z, with the complex conjugate represented by Z^*.

By examining Equations (10), we identify three terms: the desired received electrical signal $E_n(t)E_{LO}^{*}(t)$, the ICXT-LO beating term $E_x(t)E_{LO}^{*}(t)$ and the ASE-LO beating term $E_{ASE}(t)E_{LO}^{*}(t)$.

The performance of the SDM optical system represented in Figure 2 is assessed by evaluating the BER of the detected currents $I_I(t)$ and $I_Q(t)$ at the optimum sampling time instants and the OSNR penalty due to the presence of ICXT. The OSNR penalty quantifies the impact of the ICXT on the performance of the coherent receiver and is defined as the ratio between the required OSNR with ICXT that leads to a BER

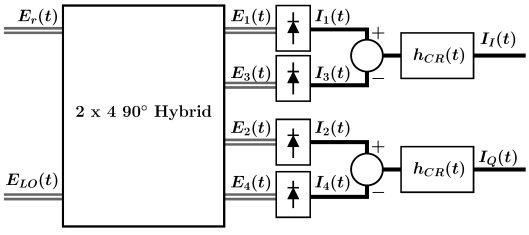

Figure 3: Model of a coherent receiver with electrical RRC filtering and ideal dispersion compensation.

of 10^{-3} and the required OSNR without ICXT for the same BER. The ICXT level that leads to a 1 dB OSNR penalty is a typical reference to evaluate the tolerance to ICXT.

3 VALIDATION OF THE ICXT TRANSFER FUNCTION

The validation of the transfer function $F(\omega)$ is performed through the comparison between the empirical estimations of the mean and variance of the amplitude of the ICXT transfer function, XTTF(ω), defined in (Cartaxo et al., 2016), and the mean and variance obtained by simulation.

The XTTF(ω) is obtained from the fluctuations after the photodetection of the crosstalk field at the output of core n, and is given by (Cartaxo et al., 2016)

$$\mathrm{XTTF}(\omega) = \frac{[F^*(0)F(\omega) + F(0)F^*(-\omega)]}{2} \tag{11}$$

Since $\mathbf{E}[|\mathrm{XTTF}(0)|] = N|K_{nm}|^2$, with $\mathbf{E}[\,]$ denoting the expected operator value. the normalized XTTF, $X(\omega)$, is defined by $X(\omega) = \mathrm{XTTF}(\omega)/\left(N|K_{nm}|^2\right)$.

The empirical expressions of the mean of the $|X(\omega)|$ is given by (Cartaxo et al., 2016)

$$\mathbf{E}[|X(\omega)|] = \left\{ x_\infty^2 + \mathrm{sinc}^2\left(\frac{\omega S_{mn}}{2\pi}\right) \left[\frac{1}{2} - x_\infty^2 + \frac{1}{2}\cos\left(\frac{LD_n\lambda^2\omega^2}{2\pi c}\right)\right] \right\}^{\frac{1}{2}} \tag{12}$$

where $x_\infty \approx 0.5549$ (Cartaxo et al., 2016) and $\mathrm{sinc}(x)$ is the sinc function, defined by $\sin(\pi x)/(\pi x)$ (Carlson and Crilly, 2009). The variance of $|X(\omega)|$ is obtained from (Cartaxo et al., 2016)

$$\mathrm{Var}\{|X(\omega)|\} = \frac{1}{2} - x_\infty^2 + \mathrm{sinc}^2\left(\frac{\omega S_{mn}}{2\pi}\right) \cdot \cdot \left[x_\infty^2 + \frac{1}{2}\cos\left(\frac{LD_n\lambda^2\omega^2}{2\pi c}\right)\right] \tag{13}$$

Figure 4 shows the comparison of the numerical simulation results for the mean and variance of the normalized XTTF amplitude with those estimated from the empirical model. The numerical simulations consider 10^5 samples of ICXT signals with $N = 1000$ PMPs, which are randomly distributed along the MCF following a uniform distribution. The parameters for the MCF are: L=25 km, λ= 1550 nm , $\Delta D_{mn} = 0$, $S_{mn} = \{25, 125\}$ ps and $D_n = \{0, 17\}$ ps/nm/km. The empirical estimations of the mean and variance of $X(\omega)$ are marked with solid lines, while the mean and variance of $X(\omega)$ obtained through simulation are shown with dashed lines. Figure 4 shows an excellent agreement between the theoretical and the simulation results for the mean and the variance of $X(\omega)$, hence, showing that the simulation model is properly implemented.

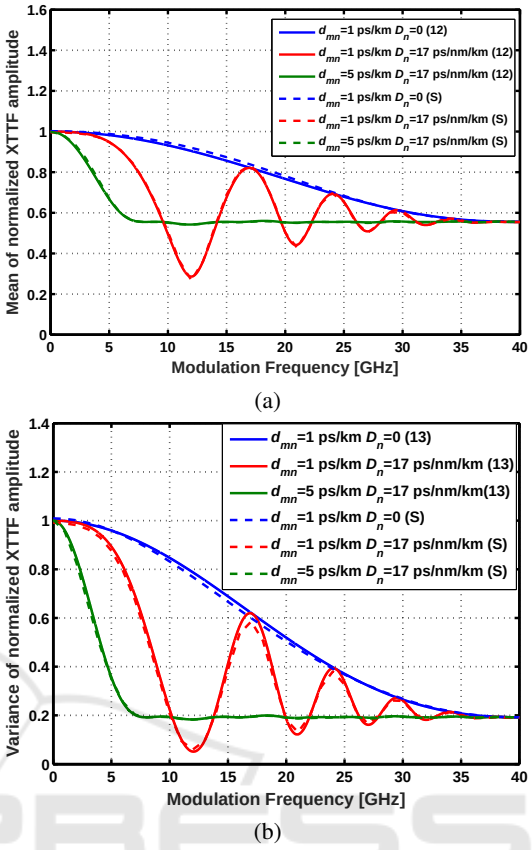

Figure 4: Comparison between the theoretical mean (Equation (12)) and variance (Equation (13)) and simulations (S) results of the (a) mean and (b) variance of the normalized XTTF as a function of the modulation frequency.

4 PERFORMANCE ANALYSIS

In this section, we assess the performance of the MCF-based SDM system with optical coherent detection using MC simulation. The performance metrics used in this work are the BER and the OSNR penalty due to the ICXT. The BER is estimated using direct error counting (DEC) and the BER is given by $N_e/(N_{it}N_sN_b)$, where N_e is the number of counted errors at the decision circuit input, N_b is the number of bits per symbol given by $\log_2(M)$, N_s is the number of simulated QAM symbols and N_{it} is the number of iterations of the MC simulation.

Table 1 presents the parameters used in MC simulation in order to assess the performance of the MCF-

Table 1: Parameters of the MCF-based SDM system.

Parameter	Value
R_b [Gbps]	56
β	$\{0, 0.25, 0.5, 0.75, 1\}$
τ_{mn}/T_s	[0, 1]
S_{mn} [ps]	[0, 35]
Modulation format	4-QAM
T_s [ps]	35.7
Number of PMPs	1000
$OSNR_0$ [dB]	10.3
Number of symbols N_s	2^{11}
Counted errors N_e	10^4

based SDM system with optical coherent detection in presence of ASE noise and ICXT. $OSNR_0$ is the required OSNR for a BER of 10^{-3} in absence of ICXT, i.e. this parameter is the reference OSNR to quantify the OSNR penalty due to the ICXT.

The validation of the simulation model of the coherent receiver presented in Figure 3 must be performed previously without ICXT. Figure 5 depicts the BER as a function of the OSNR estimated using DEC (circles) and the theoretical BER (dashed line), BER_{QAM}, as a function of the OSNR obtained using (Essiambre et al., 2010)

$$BER_{QAM} = 4\frac{(1-1/\sqrt{M})}{\log_2 M} Q\left(\sqrt{\frac{6 \cdot OSNR \cdot B_{OSA}}{(M-1)R_s}}\right) \quad (14)$$

where $Q(x)$ is the Q function, which is given by (Carlson and Crilly, 2009)

$$Q(x) = \frac{1}{\sqrt{2\pi}} \int_x^{+\infty} e^{-t^2/2} dt \quad (15)$$

B_{OSA} is the optical spectrum analyzer bandwidth, defined as 12.5 GHz (Hui and O'Sullivan, 2008) in which the OSNR is estimated, and R_s is the symbol

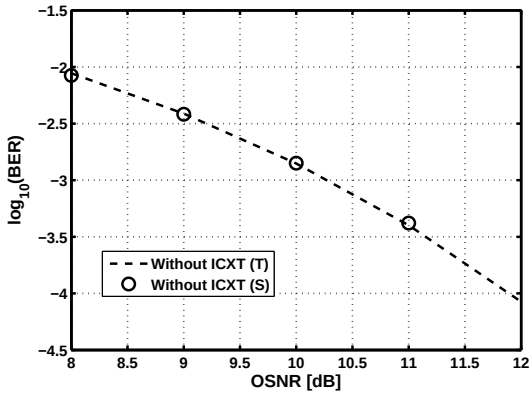

Figure 5: $\log_{10}$(BER) as a function of the OSNR obtained through simulation (circles) and theoretically (dashed line) for the 4-QAM modulation format without ICXT.

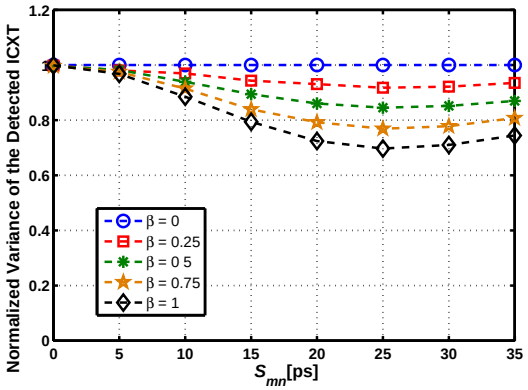

Figure 6: Normalized variance of the detected ICXT as a function of the skew, considering $\beta = \{0, 0.25, 0.5, 0.75, 1\}$ and $\tau_{mn} = 0$.

rate. From Figure 5, a perfect agreement between the DEC estimation and the theoretical BER is noticed, which validates the coherent receiver simulation model in a back-to-back configuration in presence of ASE noise and without ICXT.

In the following, we analyze the variance of the current due to the ICXT at the decision circuit input. Hence, we estimate the variance of the detected ICXT using the MC simulation, for different skews, time misalignments between the interfered and interfering core signals, and roll-off factors.

Figure 6 depicts the variance of the detected ICXT, normalized to $N|K_{nm}|^2$, as a function of the skew and the roll-off factors of 0, 0.25, 0.5, 0.75 and 1 estimated through MC simulation.

Firstly, we consider a perfect alignment between the interfered and the interfering signals, i.e. $\tau_{mn} = 0$, in order to analyze solely the influence of the skew on the ICXT variance. Figure 6 shows that the variance of the detected ICXT as a function of the skew is constant when β is 0. For higher roll-off factors, and considering $0 \leq S_{mn} \leq 35$ ps, the lowest ICXT vari-

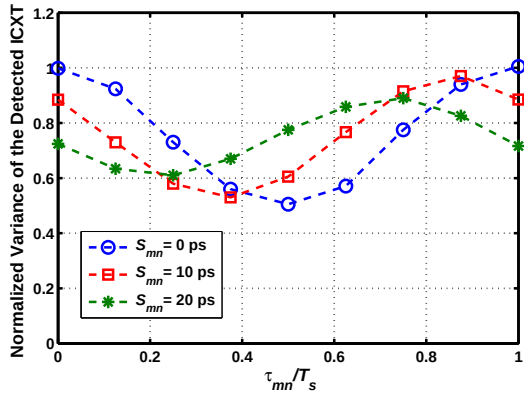

Figure 7: Normalized variance of the detected ICXT as a function of the temporal misalignment considering $\beta = 1$ and S_{mn} of 0, 10 and 20 ps.

ance is reached when the skew is 25 ps. Figure 6 also allows to conclude that the increase of the roll-factor and skew leads to a reduced ICXT variance and, consequently, lower degradation of the coherent receiver performance due to the ICXT.

Figure 7 depicts the normalized variance estimated through MC simulation as a function of the temporal misalignment between the interfered and interfering signals considering a roll-off factor of 1.

Figure 7 shows that the minimum and the maximum value of the ICXT variance are spaced by $0.5T_s$. Figure 7 also shows that the change of the skew leads to a temporal shift of the time instants that lead to the minimum and the maximum ICXT variances and also to a reduction of the difference between the maximum and minimum ICXT variances.

Next, we evaluate the penalty on the required OSNR that leads to a BER of 10^{-3} due to the ICXT. Figure 8 depicts the OSNR penalty due to the ICXT as a function of the ICXT level for the 4-QAM modulation format, considering $\tau_{mn} = 0$ and a roll-off factor of (a) 0, (b) 0.5 and (c) 1 for different values of skew. The chosen values of skew are based on the results obtained in Figure 6. The ICXT level, X_c, is defined as the ratio between the ICXT signal power and the interfered core signal power at the coherent receiver input and is given by

$$X_c = \frac{N|K_{nm}|^2 P_m}{P_n} \tag{16}$$

Figure 8(a) shows that, when the roll-off factor is 0, the variation of the skew has no influence on the OSNR penalty. This conclusion is in agreement with the results of Figure 6, since when the roll-factor is 0, the variance of the detected ICXT is independent of the skew. Moreover, Figure 8 allows to conclude that, when the interfering signal is aligned with the interfered signal, i.e. $\tau_{mn} = 0$, the OSNR penalty for a given ICXT level decreases for higher skew. For instance, in Figure 8(c), considering an ICXT level of -17 dB and $\beta = 1$, the OSNR penalty is 0.9, 0.7 and 0.6 dB for a skew of 0, 15 and 25 ps, respectively. These results are in agreement with the conclusions drawn from the analysis of Figure 6, where it is observed that the variance of the detected ICXT is lower when S_{mn} is increased. Figure 8(c) also allows to conclude that a roll-off factor of 1 and a skew of 25 ps leads to a tolerance gain to the ICXT of 1.7 dB, as the ICXT level for a 1 dB OSNR penalty with a null skew is -16.7 dB, while, for a skew of 25 ps, the ICXT level for the same OSNR penalty is -15 dB.

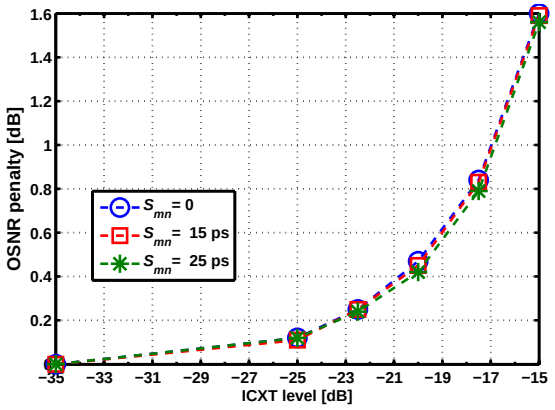

(a) $\beta = 0$.

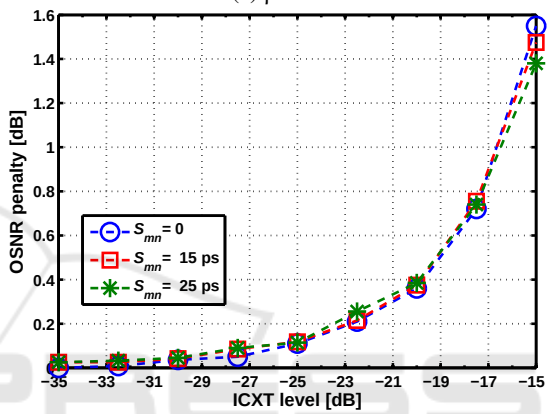

(b) $\beta = 0.5$.

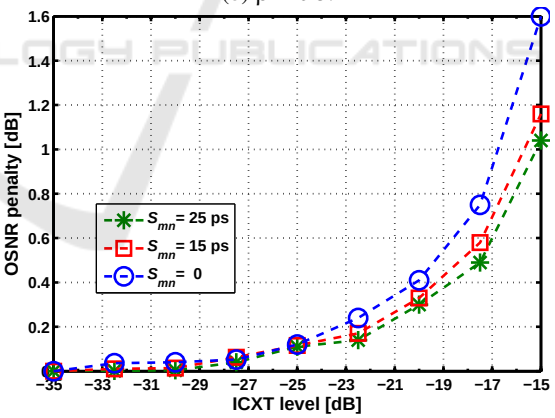

(c) $\beta = 1$.

Figure 8: OSNR penalty due to the ICXT as a function of the ICXT level considering the 4-QAM modulation format, $\tau_{mn} = 0$ and (a) $\beta = 0$, (b) $\beta = 0.5$ and (c) $\beta = 1$, and for $S_{mn} = 0$, $S_{mn} = 15$ ps and $S_{mn} = 25$ ps.

5 CONCLUSION

In this work, we assess the impact of ICXT on the BER and OSNR penalty of a MCF communication system with optical coherent detection for signals

with 4-QAM modulation. The impact is assessed for different skew between the signals transmitted in the interfered and interfering cores, different time misalignments and by varying the signals roll-off factors. To complement our results, the variance of the detected ICXT is also studied.

Our results show that the roll-off factor of the RC pulse shape and the skew has a significant influence on the variance of the detected ICXT. Considering a null roll-off factor, the variance of the detected ICXT is constant as a function of the skew. In presence of skew and with a roll-off factor higher than 0, the variance of the detected ICXT signal decreases with the increase of the roll-off factor. For a roll-off factor higher than 0 and a skew of 25 ps, the variance of the ICXT reaches its lowest value.

The temporal misalignment has also influence on the variance of the ICXT signal at the coherent receiver. Our results reveal that for a given skew, the variation of the temporal misalignment leads to a "sinusoidal" behavior of the detected ICXT variance. When the skew is reduced, the difference between the highest and the lowest variance becomes smaller. Without skew, our results reveal that the OSNR penalty is independent of the roll-off factor and the 1 dB OSNR penalty is reached with a -16.7 dB ICXT level. With skew between the cores, the ICXT level that leads to a 1 dB OSNR penalty is higher for skew of 25 ps: for $\beta = 0$, the ICXT level is -16.7 dB; for $\beta = 1$, the ICXT level for the same OSNR penalty is -15 dB, due to the reduction of the ICXT variance.

ACKNOWLEDGEMENTS

This work was supported in part by Fundação para a Ciência e a Tecnologia (FCT) from Portugal under the project of Instituto de Telecomunicações AMEN-UID/EEA/50008/2013 and the ISCTE-IUL Merit Scholarship BM-ISCTE-2016.

REFERENCES

Agrawal, G. (2010). *Fiber-Optic Communication Systems*. John Wiley & Sons, 4 edition.

Carlson, A. and Crilly, P. (2009). *Communication Systems*. McGraw-Hill, Boston, 5. ed edition.

Cartaxo, A. and Alves, T. (2017). Discrete Changes Model of Inter-core Crosstalk of Real Homogeneous Multi-core Fibers. *J. Lightwave Technol.*, 35(12):2398–2408.

Cartaxo, A. et al. (2016). Dispersion Impact on the Crosstalk Amplitude Response of Homogeneous Multi-Core Fibers. *IEEE Photon. Technol. Lett.*, 28(17):1858–1861.

Essiambre, R. et al. (2010). Capacity limits of optical fiber networks. *J. Lightwave Technol.*, 28(4):662–701.

Fini, J. M. et al. (2010). Statistics of Crosstalk in Bent Multicore Fibers. *Opt. Express*, 18(14):15122–15129.

Hayashi, T. et al. (2011). Design and Fabrication of Ultra-Low Crosstalk and Low-Loss Multi-core Fiber. *Opt. Express*, 19(17):16576–16592.

Hayashi, T. et al. (2013). Physical Interpretation of Inter-core Crosstalk in Multicore Fiber: Effects of Macrobend, Structure Fluctuation, and Microbend. *Opt. Express*, 21(5):5401.

Hayashi, T., Sasaki, T., and Sasaoka, E. (2014). Behavior of Inter-Core Crosstalk as a Noise and Its Effect on Q -Factor in Multi-Core Fiber. *IEICE Trans. Commun*, (5):936–944.

Hui, R. and O'Sullivan, M. (2008). *Fiber Optic Measurement Techniques*. Elsevier Academic Press.

Jeruchim, M., Balaban, P., and Shanmugan, K. (2000). *Simulation of communication systems: modeling, methodology and techniques*. Kluwer Academic Publishers, Norwell, MA, 2nd edition.

Klaus, W. et al. (2017). Advanced Space Division Multiplexing Technologies for Optical Networks. *J. Opt. Commun. Netw.*, 9(4):C1–C11.

Morioka, T. (2017). High-Capacity Transmission Using High-Density Multicore Fiber. In *Optical Fiber Communication Conference*, page Th1C.3.

Puttnam, B. J. et al. (2015). 2.15 Pb/s Transmission Using a 22 Core Homogeneous Single-Mode Multi-Core Fiber and Wideband Optical Comb. In *European Conference on Optical Communication (ECOC)*, pages 1–3.

Puttnam, B. J. et al. (2017). High Capacity Transmission Systems Using Homogeneous Multi-Core Fibers. *J. Lightwave Technol.*, 35(6):1157–1167.

Rademacher, G. et al. (2017a). Crosstalk Dynamics in Multi-Core Fibers. In *Opt. Express*, pages 12020–12028.

Rademacher, G. et al. (2017b). Time-Dependent Crosstalk from Multiple Cores in a Homogeneous Multi-Core Fiber. In *Optical Fiber Communications Conference and Exhibition (OFC)*, pages 1–3.

Saitoh, K. and Matsuo, S. (2016). Multicore Fiber Technology. *J. Lightwave Technol.*, 34(1):55–66.

Takara, H. et al. (2012). 1.01-Pb/s (12 SDM/222 WDM/456 Gb/s) Crosstalk-managed Transmission with 91.4-b/s/Hz Aggregate Spectral Efficiency. In *European Conference and Exhibition on Optical Communication (ECOC)*, page Th.3.C.1.

Xia, T. and Wellbrock, G. (2013). Commercial 100-Gbit/s Coherent Transmission Systems. In *Optical Fiber Telecommunications*, chapter 2, pages 45 – 82. Academic Press, Boston, 6 edition.

Zhu, B. et al. (2011). 112-Tb/s Space-Division Multiplexed DWDM transmission with 14-b/s/Hz Aggregate Spectral Efficiency over a 76.8-km Seven-Core Fiber. *Opt. Express*, 19(17):16665–16671.